Direct observation of liquid-liquid phase coexistence in deeply supercooled water using an accurate polarizable multipole model

Lee-Ping Wang

leeping@ucdavis.edu

University of California, Davis https://orcid.org/0000-0003-3072-9946

Margaret Berrens

University of California, Davis

Davide Donadio

University of California Davis https://orcid.org/0000-0002-2150-4182

Physical Sciences - Article

Keywords:

Posted Date: August 16th, 2024

DOI: https://doi.org/10.21203/rs.3.rs-4650185/v1

Additional Declarations: There is **NO** Competing Interest.

Direct observation of liquid-liquid phase coexistence in deeply supercooled water using an accurate polarizable multipole model

Lee-Ping Wang,* Margaret T. Berrens, and Davide Donadio

Department of Chemistry, University of California Davis, Davis, CA, 95616

E-mail: leeping@ucdavis.edu

Abstract

Liquid water can be supercooled up to about 50 K below the melting point before undergoing homogeneous ice nucleation. Based on experimental thermodynamic observations and computer simulations it was hypothesized that below this temperature and at pressures of several kbar water undergoes a liquid-liquid phase transition (LLPT) and the transition line ends at a second critical point. However, challenges in experiments and simulations at such deep cooling leave doubts about the nature of the LLPT and the existence of the critical point. Here we use molecular dynamics simulations with a highly accurate and computationally efficient polarizable water model to establish the character of the LLPT and identify the location of the second critical point. Our microsecond-long simulations provide the first direct evidence of a well-defined moving interface between low-density and high-density water at conditions near the phase boundary. This is the ultimate proof of a first-order transition between two liquid phases with distinct free energy basins separated by a barrier, resolving a long-standing

debate. These results provide new perspectives on supercooled water under pressure simulated with an accurate and realistic model suitable for studies of water in confined geological and biological environments.

Introduction

Water is the quintessential solvent of life on Earth and one of the most well-studied compounds in Nature, yet it still has many unknown properties. Over decades, one question that has attracted much attention is how liquid water behaves under deeply supercooled and pressurized conditions. Experiments conducted below 130 K showed that glassy metastable water exhibits polyamorphism, with three phases, low-, high- and very-high-density amorphous ice (LDA, HDA, VHDA), the first two being likely separated by a first-order phase transition.[1,2] A new form of medium-density amorphous ice was recently discovered.[3] The continuation of the phase boundary line between LDA and HDA above the water glass temperature has prompted the conjecture of a liquid-liquid phase transition (LLPT) between a low-density liquid (LDL) and a high-density liquid (HDL) with a liquid-liquid critical point (LLCP) occurring below the homogeneous nucleation temperature ($\sim$ 235 K).[4,5]

The tendency of supercooled water to rapidly recrystallize hinders experiments in the temperature range between 130 and 235 K so that this thermodynamic region is named *no man's land*.[6,7] Nevertheless, recent experiments using femtosecond X-ray pulses applied to supercooled microdroplets[8,9] and transiently heated amorphous ice revealed structural information consistent with the phase separation hypothesis.[10–12]

Since the LLPT hypothesis was proposed, computer simulations have been extensively employed to resolve the nature of the LLPT of water in no man's land. In particular, these studies rely on molecular dynamics (MD) simulations of water models of various complexity to assess the existence and the location of the LLCP. Until very recently, simulation efforts have focused on rigid, fixed-point-charge water models, such as the landmark ST2 model[13–15] or the TIP4P-2005 and TIP4P-ice models.[16–18] Despite the simplicity of these

models, simulating the LLPT has been extremely challenging due to the sluggish dynamics of supercooled water and the large fluctuations occurring in the proximity of a phase boundary. The rigorous proof of the LLPT requires delicate free energy calculations that need long equilibration times and meticulous finite-size convergence studies. Hence, a consensus on the first-order nature of the LLPT of the ST2 water model was reached only after a long heated debate.[19–21] Remarkably, the nature of the phase transition for TIP4P models remains debated, with early evidence in favour of a first-order LLPT[22] seemingly contradicted by more recent calculations, which did not find any free-energy barrier separating LDL and HDL.[23]

Several complex water models with more realistic physical features, such as bond flexibility and polarization effects, exhibit signatures of LLPT.[24–26] Among them, it is worth mentioning a deep neural network (DNN) model fitted to density functional theory calculations using the SCAN exchange and correlation functional, for which direct simulations and free energy calculations suggest the existence of a first-order LLPT with a second critical point.[27] However, as in the case of TIP4P/2005, these results may be biased by the limited size of the models ($\sim$ 500 molecules in the cited studies). In small systems, direct simulations may not distinguish whether a temperature-driven transition is first-order or higher-order, and enhanced-sampling calculations may be biased as well.[28] Additionally, in several cases, MD simulations up to several hundred ns are not long enough to probe the slow dynamics of systems at temperatures below 200 K. To circumvent this issue, the LLPT is usually inferred from the low-temperature extrapolation of a thermodynamic model fitted to MD data at higher temperatures.[22,25] Size-independent direct evidence of a first-order LLPT, such as a moving interface between LDL and HDL, has not been provided especially for complex computationally intensive models. Ultimately, even the most sophisticated models entail significant discrepancies with real water: for example, the melting temperature of ice I_h at ambient pressure with DNN-SCAN is 308 K (35°C).[29] Overall, previous works suggest that the existence of a first-order LLPT and the location of the second critical point depend strongly on the approximations of the water model, limitations in the simulation cell size,

and details of the enhanced sampling algorithms.

In this work, we probe the LLPT in supercooled water using a highly accurate, yet computationally efficient water model, which enables very long (10 μs) simulations with large system sizes (8,000 atoms), together with new analysis methods that can effectively distinguish between the two proposed liquid phases. We employ a flexible all-atom polarizable machine-learning model, iAMOEBA (Inexpensive Atomic Multipole Optimized Energetics for Biomolecular Applications). iAMOEBA uses a sophisticated model for nonbonded interactions including atom-centered permanent charges, dipoles and quadrupoles, and "direct" induced point dipoles that approximate the full N-body polarization energy as a 3-body interaction, enabling iAMOEBA to be significantly faster than the AMOEBA polarizable model upon which it is based. The parameters of iAMOEBA are trained on a comprehensive dataset that includes both high-level *ab initio* calculations and thermodynamic properties of liquid water. Validation studies of the iAMOEBA model showed its high accuracy in predicting experimental thermodynamic, structural and dynamic data outside the training set (Table S1 and Ref. 30); for example, the ice Ih melting point, shear viscosity and self-diffusion activation energy were predicted to within 5% of experiments, and the computed phase diagram identifies five ice phases (Ih, II, III, V, VI) in the correct relative positions, indicating a high degree of suitability for investigations of supercooled water. Recent X-ray scattering experiments on supercooled liquid water down to 227 K also showed an excellent agreement with iAMOEBA predictions of the temperature dependence of structural parameters.[31,32]

The primary evidence for an LLPT in our study is derived from novel phase coexistence simulations of LDL/HDL liquids. These two-phase simulations are prepared by an LDL and an HDL model in direct contact, then tracking the evolution of the phase boundary, defined through a physically motivated order parameter that discriminates between HDL and LDL phases. The new order parameter, called "second solvation shell intruders" (SSSI), counts the number of water molecules that are spatially close to the target molecule but separated by > 2 hydrogen bonds, thereby quantifying the local density and distortion of the network.

Using the order parameter to classify molecules as HDL- or LDL-like, followed by an analysis of the interface roughness, the time evolution of the HDL-LDL interface can be observed and the interfacial tension may be measured - based on interfaces that remain stable for > 100 ns we can estimate an interfacial tension of 6 - 10 mJ m^{-2} between the two liquid phases. This work provides a new perspective on the possibility of a LLPT in a realistic water model and a new computational strategy for interrogating the phase boundary that complements published free energy simulation approaches.

Results

The thermodynamic landscape of supercooled iAMOEBA water.

We first computed the temperature and pressure dependence of the thermodynamic properties of iAMOEBA water using a large set of bulk simulations with 500 water molecules at more than 100 different T/P conditions. Many of these simulations exceeded 2 μs in length (Figure S1). Based on analysis of the thermodynamic properties (Figure 1 and Figure S2), the liquid-liquid phase transition line of the iAMOEBA water model likely resides below 188 K and above 1600 atm. In this region, the simulated density drops precipitously with decreasing temperature, the thermodynamic response functions become very large, and the liquid also becomes dramatically more structured (Figure S3). In particular, large fluctuations of the density in excess of 10% were observed for simulations performed at 188.15 K and 1600 atm (Figure S4), which we took as our best estimate of the proposed critical point.

Dynamical heterogeneity in supercooled iAMOEBA water simulations with bimodal characteristics.

The dynamical heterogeneity of supercooled water has been observed in simulations[33] as well as experiment,[34] and simulations have predicted that ice nucleation can be initiated from low-mobility regions in supercooled water.[6] Herein, our MD simulations of iAMOEBA water

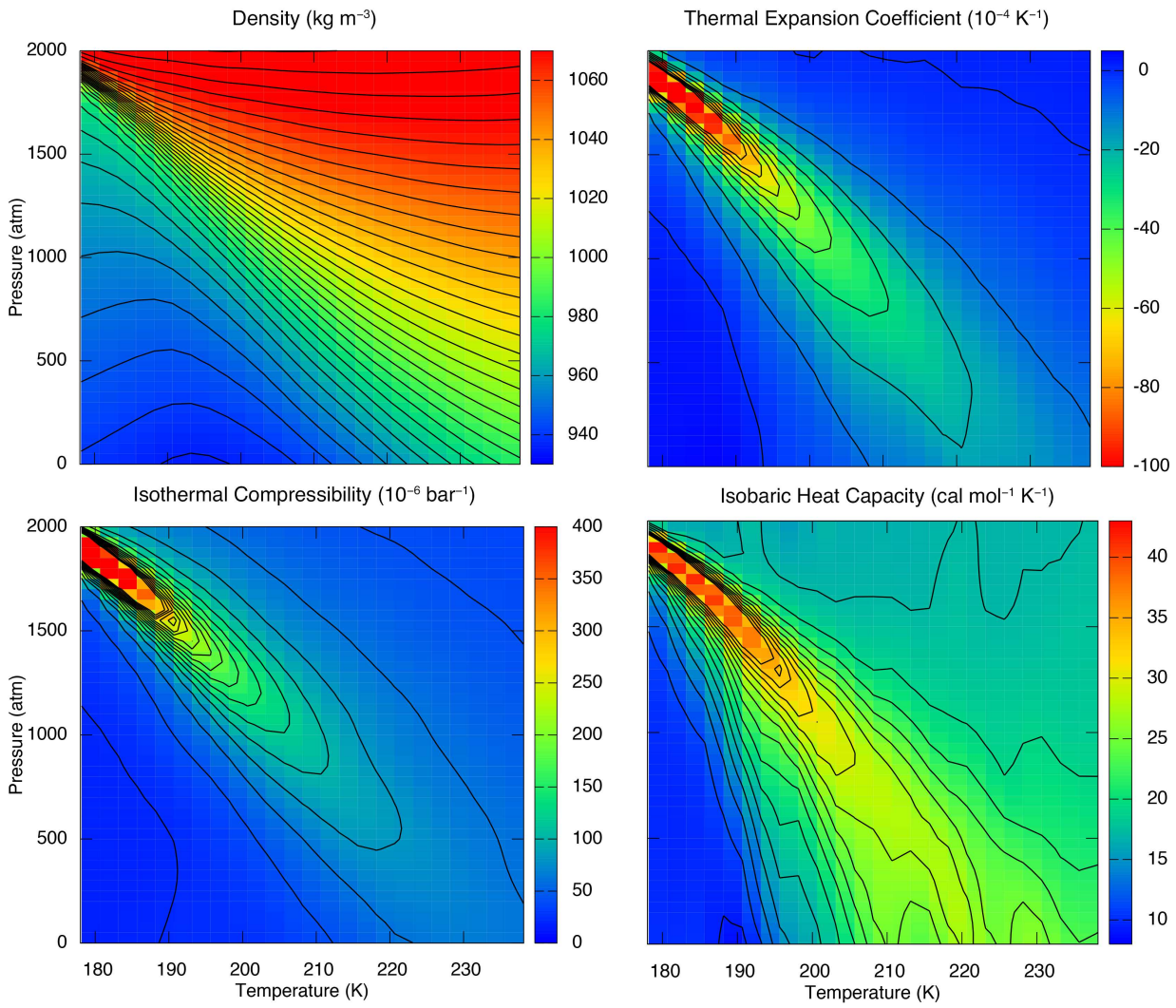

Figure 1: Thermodynamic properties of supercooled water computed using the iAMOEBA model showing the apparent divergence in the temperature and pressure dependence of the density at $T < 188$ K and $P > 1600$ atm. This data is also shown using line plots in Figure S2.

near the proposed critical point also feature a dramatic degree of dynamical heterogeneity that spans the entire simulation cell. To characterize the dynamical properties, we plot time-dependent histograms of the per-molecule diffusion coefficient, which is calculated as:

$$D_i(t, \Delta t) = \frac{|\mathbf{r}(t + \Delta t) - \mathbf{r}(t)|^2}{\Delta t} \tag{1}$$

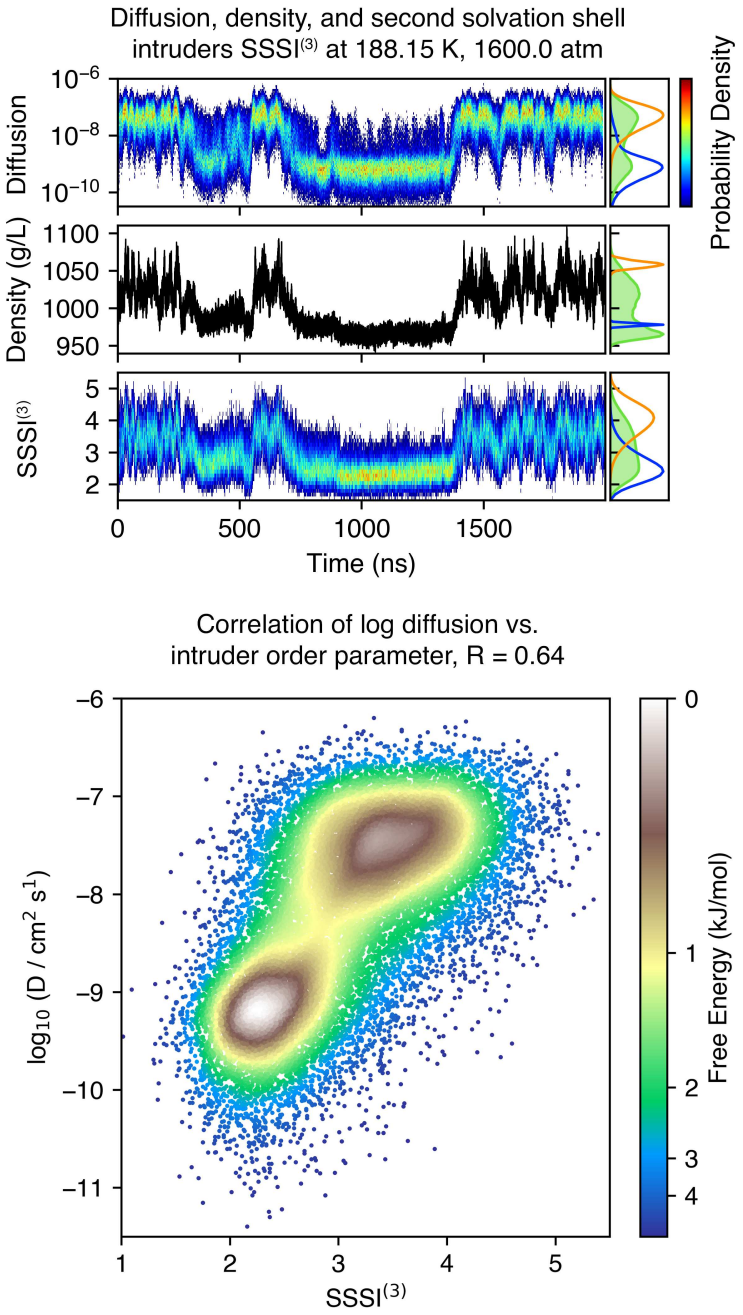

Figure 2: Top: Time series plot of the distribution of per-molecule diffusion coefficients (top), density (middle), and SSSI$^{(3)}$ order parameter (bottom). The details of SSSI are described in the main text. The properties indicate the simulation fluctuates between two qualitatively different regimes, which is consistent with the interpretation of two liquid phases. Bottom: Scatter plot of the log per-molecule diffusion coefficient vs. the SSSI$^{(3)}$ order parameter for the same simulation. The observation of good correlation ($R = 0.64$) shows that SSSI is a good order parameter for distinguishing between the kinetically distinct regimes. This is a 2 μs segment of a 10 μs trajectory corresponding to 3-5 μs; the full analysis is shown in Figure S4.

where the numerator measures the squared displacement of the oxygen atom of water molecule i over the lag time Δt, here chosen to be 10.0 ns. This quantity gives the bulk diffusion coefficient when averaged over all molecules in the liquid phase. We observed strong non-Gaussian behaviour in the distribution with signatures of bimodality, characterized by large fluctuations between a fast and slow regime where the mean per-molecule diffusivity differs by 2-3 orders of magnitude. A time series plot of the simulated density at 188.15 K, 1600.0 atm using a cubic box of 500 molecules shows that changes in the diffusivity distribution are accompanied by fluctuations in the bulk density (Figure 2 upper). Simultaneous plotting of the bulk density together with the s_2 order parameter (the pairwise contribution to the excess entropy, a measure of the local fluid structure) shows that a small free energy barrier exists between two minima corresponding to the HDL and LDL phases; however, only one free energy minimum is observed when the same analysis is performed on a simulation cell containing 1000, 2000, or 4000 molecules (Figure S5). This is consistent with prior studies that note the tendency for smaller system sizes to enhance apparent two-phase behaviour,[19,28] and provides motivation for simulating the liquid-liquid interface by construction.

A structural basis for observed anomalies in kinetic properties.

A thermodynamic phase represents a domain of configuration space and thus cannot be distinguished by kinetic properties alone. The search for an order parameter that can distinguish between two liquid phases has been extensively reported in the literature, with the publication of increasingly advanced order parameters in recent years including with the aid of machine learning.[35–39] Here we describe a new and simple order parameter called "second solvation shell intruders" (SSSI) which is defined as the number of water molecules in the second solvation shell that are not included in the first solvation shells of molecules in the first solvation shell. Define $S_{i;n}$ as the set of n closest water molecules to molecule i. The

SSSI for molecule i is defined as

$$\mathrm{SSSI}(i) \equiv \left| S_{i;16} - \bigcup_{j \in S_{i;4}} S_{j;4} \right| \tag{2}$$

SSSI is based on the evidence that in higher-density phases of water, albeit remaining tetrahedrally coordinated, each water molecule has an increased number of neighbouring molecules that penetrate between the first and second solvation shells but are not directly hydrogen bonded. In the limiting case of ordinary ice Ih, the hydrogen bonding network is relatively open and characterized by hexagonal hydrogen-bonded rings; as a result, the molecules that are separated by a greater number of hydrogen bonds are also more spatially distant. By spatially distorting this network, molecules with a larger H-bond degree of separation can enter the spatial voids of the network, thus "intruding" into the second solvation shell.[40]

The SSSI takes integer values between 1 and 6 for the phases being studied and has only a weak correlation with the diffusion coefficient. To take into account longer-range effects, we define the solvation shell-averaged $\mathrm{SSSI}^{(n)}$ as:

$$\mathrm{SSSI}^{(n)}(i) \equiv \frac{1}{5} \left(\mathrm{SSSI}^{(n-1)}(i) + \sum_{j \in S_{i;4}} \mathrm{SSSI}^{(n-1)}(j) \right) \tag{3}$$

where $\mathrm{SSSI}^{(0)} \equiv \mathrm{SSSI}$ as defined in Eq. 2 and $\mathrm{SSSI}^{(1)}$ averages the values of $\mathrm{SSSI}^{(0)}$ over the five molecules within the first solvation shell including the target molecule at the centre. The averaging process may be repeated up to any desired n to include contributions from more distant neighbours (here we adopt $n = 3$). We find that $\mathrm{SSSI}^{(3)}$ has an excellent correlation with the per-molecule diffusion coefficient (Figure 2 lower), and this result holds over multiple simulations at different thermodynamic conditions (Figure S6), making it a good choice to investigate the time evolution of the liquid-liquid interface in the next section.

Simulating the liquid-liquid interface.

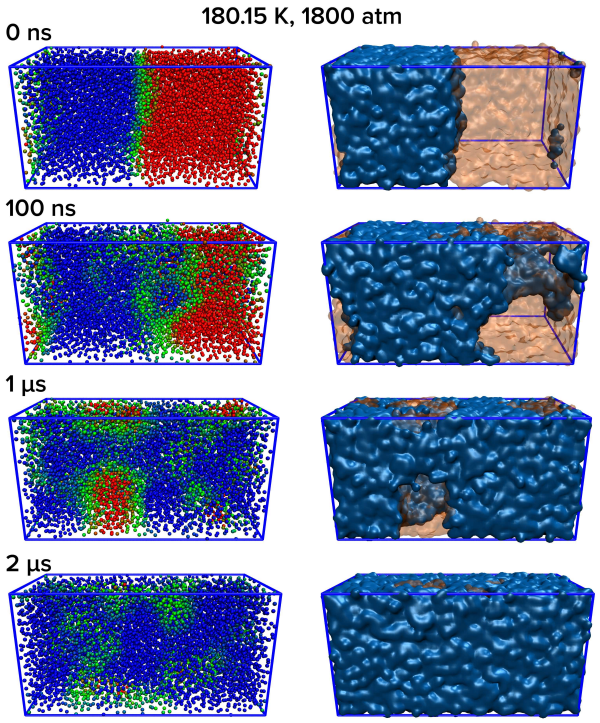

Figure 3: 3-D renderings of water oxygen atoms for a simulated HDL/LDL interface with 8000 molecules at 180.15K, 1800 atm. Left: Atoms are coloured by the intruder order parameter, using a colour scale from 2.5 (blue, LDL) to 3.5 (red, HDL). Right: Surfaces are drawn corresponding to regions with the intruder order parameter < 3.0 (blue) and > 3.0 (orange transparent). Indicate LDL and HDL in the figure. This simulation is not on any PT map. Would it make sense to have a series of snapshots where HDL wins in the same figure?

The hypothesis of a first-order LLPT implies that a coexistence line separates the HDL and LDL phases for $T < T_c$ and $P > P_c$ where (T_c, P_c) corresponds to the hypothetical liquid-liquid critical point (LLCP). In a two-phase simulation started from HDL and LDL phases in contact and thermodynamic conditions close to the phase transition line, one should expect to observe two metastable phases with a moving interface.[41–44] The number of molecules in each phase is expected to change until only one phase remains, depending on whether the simulation conditions are located on the HDL or LDL side of the phase transition line. Moreover, because a first-order phase transition implies two thermodynamically stable phases, there should be a free energy cost involved in creating the interface, which limits the

interfacial area.

Here we use the $SSSI^{(3)}$ order parameter with a threshold of 3.2 to discriminate between the two phases, given the good correlation with the log diffusion coefficient and bulk density determined above. For a simulation initiated with 50% HDL and 50% LDL on the high-T high-P side of the phase coexistence line, one should expect to see the HDL-LDL interface move toward the LDL side, eventually resulting in the complete conversion to the 100% HDL phase (and conversely, conversion to 100% LDL on the low T, low P side).

To set up a simulation that initially consists of 50% HDL and 50% LDL, a pair of configurations was taken from constant-pressure simulation trajectories at HDL and LDL conditions respectively, in which the cross-sectional areas were set to the same value for both simulations while allowing the barostat to modify the C axis. The two configurations were then stacked normally to the C-axis with a small (3 Å) separation to create a configuration of a two-phase system containing a total of 8000 molecules (Figure 3 top). Figure 3 shows snapshots from a trajectory at 180.15 K, 1800 atm. After 100 ns of simulation, a greater number of molecules have assigned lower values of $SSSI^{(}3)$ corresponding to the LDL phase. In this snapshot, the two interfaces are connected by a "channel" of LDL water molecules that extend across the HDL domain on the right. After 1 μs, most of the molecules are now in the LDL phase and only small pockets of the HDL phase remain. We determined these conditions to be on the LDL side of the phase coexistence line, while simulations that used a slightly higher pressure (180.15K, 2000 atm) or temperature (182.15K, 1800 atm) transitioned toward the HDL side on a similar $\sim$ 100 ns timescale.

Analysis of liquid-liquid interfacial area and interfacial tension.

To establish whether there is a stable liquid-liquid interface, we carried out a clustering analysis of the simulation trajectories to determine the number of molecules at the interface as a function of time. A snapshot of the starting configuration is shown in Figure 4, along with a histogram of the $SSSI^{(}3)$ values for two simulations at equilibrium in their respective

LDL and HDL phases. Blue corresponds to LDL and orange to HDL. Using a threshold of 3.2 determined by the crossover point of the two histograms, the molecules were classified as either HDL or LDL, and clustering was performed using a distance cutoff of 3.4 Å. The largest cluster for each phase was identified, and the molecules at the interface were defined using the number of neighbours in the same cluster within 3.4 $\mathring{A}$ of the central atom; if that number was less than 4, then the atom was considered an interfacial atom. For the system titled 'LDL' corresponding to conditions of 174.15 K and 1800.0 atm, the biggest cluster of the LDL phase expands until it includes almost the entire system whereas the size of the biggest cluster of the HDL phase goes to zero. We then see the opposite trend for the system titled 'HDL' corresponding to 180.15 K and 2000.0 atm. For both systems, we see the presence of an interface where the number of interfacial molecules is clearly bounded ($\leq$25 % of all molecules in the system) until one phase takes over and the interface size drops close to zero molecules. For the third system titled 'supercritical', corresponding to 198.15 K and 1200.0 atm, the analysis results in an evenly distributed mixture of the two phases for all times. The number of interfacial molecules increases to 5000-6000 (nearly 75% of all molecules in the simulation), and a significant number of molecules (2000-3000) are assigned to clusters other than the two largest. The analysis shows that the first two simulations on either side of the LLPT line are characterized by a single HDL domain and a single LDL domain separated by a well-defined interface, whereas the phases are clearly not separated at the supercritical conditions.

The interface between distinct phases is not perfectly flat due to thermal fluctuations. Using capillary wave theory, these fluctuations can be related to the interfacial tension in the following way:

$$\gamma \equiv \frac{k_B T}{2\pi \langle \sigma^2 \rangle} \ln \frac{L}{\xi} \tag{4}$$

where k_B is the Boltzmann constant, T is the absolute temperature, L is determined by the size along the x- or y- dimension (assuming z is normal to the surface) and ξ is the the bulk correlation length.[45] Using this relationship we are able to estimate the interfacial

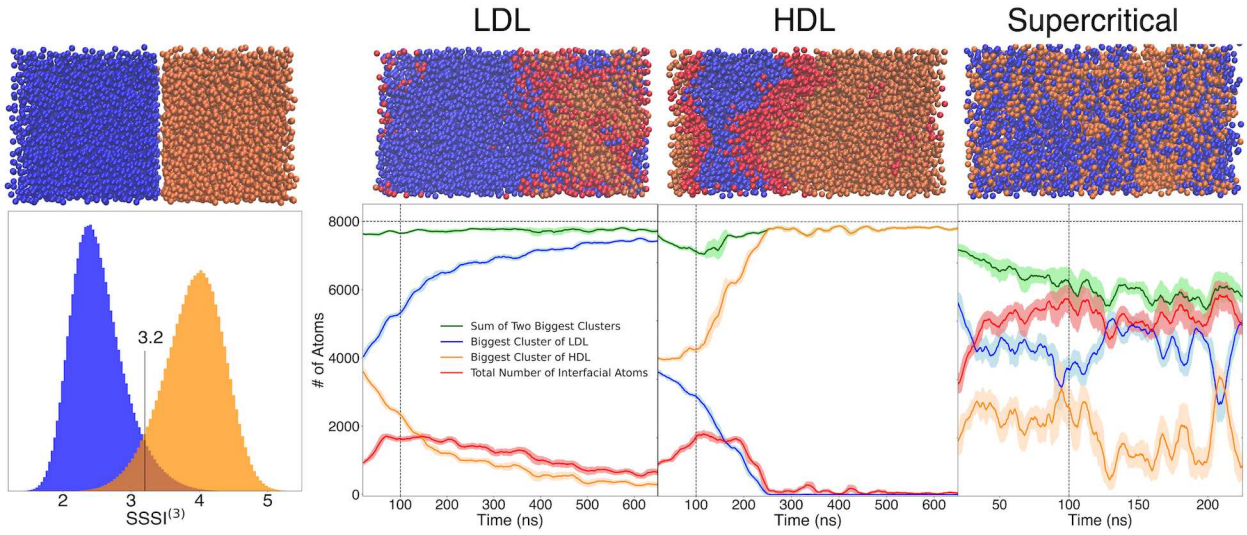

Figure 4: Left: Histogram of $SSSI^3$ values for a simulation at 180.15K-1800.0 atm after 1500 ns in the LDL phase at equilibrium (blue) and 184.15K-1800.0atm after 300 ns in the HDL phase at equilibrium (orange) plotted with a 3-D rendering of the starting frame for all coexistence simulations where atoms are colored to their corresponding phase. Right: Number of atoms for a given group versus time, plotted with a 3-D rendering of an extracted from (time point indicated by the dashed vertical line) of water oxygen atoms for simulated HDL/LDL interfaces with 8000 molecules. Clusters are determined to be for a certain phase with the threshold 3.2. Atoms are colored according to their phase. The red line represents the total number of atoms identified as an interfacial atom. The green line corresponds to the sum of the atoms in the biggest clusters for each phase at each time point. Left: 174.15 K-1800.0 atm Middle: 180.15 K - 2000.0 atm Right: 198.15 K - 1200.0atm.

free energy between the LDL and HDL supercooled phases of water, using our coexistence MD simulations previously described. We set $L = 49.95$ $\mathring{A}$ according to our simulation cell size, and $\xi = 3.5$ $\mathring{A}$ corresponding to the first minimum of the radial distribution function of water. The mean squared fluctuation of the molecules located at the interface is calculated as: $\langle \sigma^2 \rangle \equiv \langle (z - \langle z \rangle)^2 \rangle$ where we selected molecules from the largest LDL cluster belonging to one of the two interfaces in the periodic cell. The calculation is stopped when the selected interface becomes locally vertical (i.e. approximate tangent plane contains $\hat{z}$) or comes into contact with the other interface.

Figure 5 shows the interfacial tension estimated for 6 different coexistence simulations, two of which were carried out under supercritical conditions with respect to the proposed phase diagram. For simulations A, B, C, and D, a flat interface is present for approximately

281, 154, 27, and 70 ns respectively. For simulations E and F, a flat interface vanishes within 5 ps due to the simulations being carried out under supercritical conditions. Therefore, we were only able to estimate the interfacial tension for simulations A, B, C, and D. Based on each of these simulations the interfacial tension is estimated to have an average value of 7.813 $\pm$ 1.192 mJm^{-2} (Figure 5 ii) which is approximately one order of magnitude smaller than the surface tension of water and four times smaller than the estimated interfacial tension of the ice-water interface.[46] Figure 5 iii) shows how for the two sampled simulations carried out under the proposed supercritical conditions the surface roughness almost immediately jumps to high values indicating the lack of a stable flat interface. Conversely, for a simulation such as D, which was carried out under conditions near the coexistence line, the roughness remains at a constant value for 70 ns indicating the presence of a flat interface.

Discussion

To demonstrate evidence of a phase transition, one must present evidence of two free energy minima. Our homogeneous phase simulations of supercooled iAMOEBA water indeed exhibited two free energy minima separated by a small free energy barrier at conditions close to the apparent critical point (Figure S5). However, this effect became less pronounced or disappeared entirely for larger system sizes, illustrating the tendency for finite-size effects to magnify apparent phase transition behaviour.[28] As the system size increases, one needs to sample the free energy surfaces at lower temperatures to see separate minima, implying even longer runs and higher computational costs. This problem may be circumvented by performing enhanced sampling simulations that include biases in the potential energy surface or the initial conditions, but these simulation results depend on the choice of the reaction coordinates to construct the bias potential, which can be highly nontrivial. Our approach, instead, is based on the idea that the existence of 2 free energy minima implies there is a free energy cost to creating an interface between the two phases in contact, and therefore,

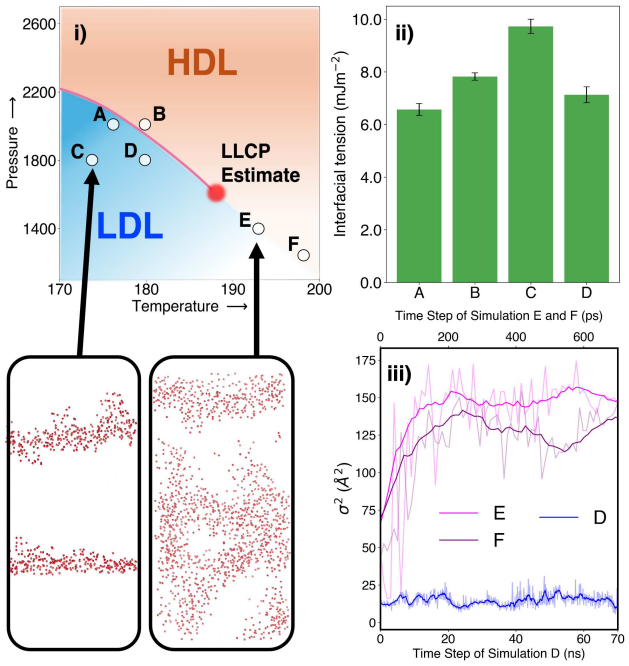

Figure 5: Estimation of the Interfacial Surface Tension (mJm^{-2}) between the low and high-density supercooled phases of water as a function of temperature and pressure. i) Phase diagram where markers represent the thermodynamic conditions for the coexistence trajectories labeled A, B, C, D, E, and F which were used to estimate the interfacial tension. The images represent the identified interfacial atoms for a given frame from the identified trajectories ii) Estimates of the interfacial tension averaged over the duration of time where a flat interface is present with respect to each trajectory (A, B, C, and D) iii) Moving average of the surface roughness versus time for trajectories E, F (window size 70 ps), and D (window size 1 ns).

a simulation of phase coexistence is a viable alternative to applying biases in single-phase simulations. This is done routinely to determine the melting point of solids.[29] By tracking the interfacial roughness over time, we can estimate the interfacial tension, and, as long as the interfacial tension takes a nonzero value, the hypothesis of two liquid phases is substantiated. To track the time evolution of the interface, global order parameters such as density and S2 are insufficient and a local order parameter is needed that correlates well with the distinct characteristics of the two phases. The SSSI is a physically motivated and simple order parameter that serves this purpose due to its good correlation with both the self-diffusion coefficient and the density.

Due to the low interfacial tension at the simulated conditions, likely owing to the prox-

imity to the LLCP, the interface deviates significantly from ideal flatness. Our approach for calculating interfacial tension requires a unique value of the interfacial z position for a given (x, y) coordinate, and can no longer be used when any portion of the interface becomes perpendicular to the xy-plane. Moreover, our coexistence simulations, which contain two liquid-liquid interfaces by construction, always collapse to one phase when the two interfaces touch one another, whether this is due to a thermodynamic driving force or a random fluctuation (in all of our simulations, this happens within < 2 μs). Therefore, we think it should be possible to measure the interfacial tension for longer times than we were able to demonstrate here using alternate approaches for calculating interfacial areas[47] and further increasing the simulation cell sizes.

Conclusion

The structure and dynamics of deeply supercooled water are characterized by long correlation lengths and slow time scales making it challenging to obtain computational insights into whether a liquid-liquid phase transition exists. Simulations of supercooled water require a large number of molecules to minimize finite-size effects and long simulation times to observe slow dynamical processes, while also being sufficiently accurate to make predictions for real water. With modern computational resources, researchers are always faced with the decision of "accurate potentials, large sizes and long times: choose two". Our present study stands out by attempting to strike a near-ideal balance of these three aspects. The iAMOEBA model is capable of predicting experimental observables of supercooled water with excellent accuracy (as well as liquid, water, and ice properties over many temperatures and pressures), and is also computationally inexpensive enough to reach multi-μs time scales with simulation cells containing nearly 10,000 molecules using open-source software running on inexpensive GPUs.

Our simulation setup was designed to directly investigate the existence of two-phase be-

haviour by starting from a synthetic interface between liquids simulated at HDL/fast and LDL/slow conditions followed by analyzing the trajectories with an order parameter that efficiently classifies molecules into either phase based on their local coordination environments. At temperatures and pressures around 180 K, 1800 atm, a metastable interface is observed for > 100 ns with a measurable interfacial tension, providing evidence for the existence of two metastable liquid phases; on the other hand, at slightly higher temperatures and lower pressures (193 K, 1400 atm), the interface vanishes nearly instantly (< 10 ps) with no measurable interfacial tension. These observations support a first-order LLPT that terminates in a critical point near 188 K, 1600 atm, corresponding to conditions where we observed the largest fluctuations in density and the highest values of thermodynamic response functions in bulk simulations.

This work contributes to a growing body of evidence for the existence of a first-order LLPT in realistic water models,[22,24–27] which implies the phenomenon may one day be unambiguously observed in real water. Future computational and experimental studies may also reveal LDL-like and HDL-like structures in supercooled water at higher temperatures above the LLCP, or in biological and geological environments where freezing is suppressed by confinement.[48–52]

Methods

The MD simulations in this study used the iAMOEBA[30] polarizable force field for water. iAMOEBA uses a direct polarization approximation in which the induced dipoles are solely determined from electric fields of the permanent multipoles and does not include mutual induction between induced dipoles. This approximation allows iAMOEBA to skip the computationally expensive step of solving for the fully self-consistent mutual polarization and significantly reduces the cost compared to the full AMOEBA model (though, the cost of the mutual polarization can be mitigated by other approaches[53–57]) The initial conditions are

periodic cells, cubic or tetragonal, containing 500 to 8000 molecules. Constant temperature conditions were simulated using a Langevin dynamics approach, integrated using a multiple time-step velocity Verlet algorithm with velocity randomization (MTS-VVVR).[58] In this multiple time-stepping scheme, the force contributions from the bonded degrees of freedom were evaluated at a "fast" 0.5 fs interval, whereas the nonbonded interactions (electrostatic, polarization, and vdW) were evaluated at a "slow" 2.0 fs interval. The particle mesh Ewald approach was used to perform long-range summation of electrostatic interactions[59] with a real-space cutoff of 7.0 Å and a grid spacing of approximately 1.0 Å corresponding to a $30 \times 30 \times 30$ grid for a 500-molecule cubic box, and $60 \times 60 \times 120$ for a 8000-molecule tetragonal box. The Van der Waals interactions used a cutoff of 9.0 Å and an isotropic long-range tail correction. The Langevin equation was used for temperature control, with a collision frequency set to 0.1 ps^{-1} in order to minimize the effects of the thermostat on kinetic properties.[60] A Monte Carlo barostat was employed to sample the isothermal-isobaric ensemble with an attempt frequency of 25 steps (50 fs). All MD simulations were carried out using the OpenMM software package, version 7.4.1.[61]

Acknowledgement

L.-P. W. thanks Jonas Sellberg, Lars Pettersson, Anders Nilsson, T.J. Lane, and Christian Schwantes for helpful discussions. D.D. and M.B. acknowledge support from NSF award 2053235.

Author contributions

L.-P. W. designed the study, performed the simulations, conceptualized and performed data analysis, authored the figures, and wrote the manuscript. M.B. performed data analysis, authored the figures, and wrote the manuscript. D.D. designed the study, conceptualized the data analysis, and wrote the manuscript. All authors contributed to scientific discussions,

interpretation of data, and revising the manuscript.

Competing interests

The authors declare no competing interests.

Supporting Information Available

The Supplementary information contains plots of thermodynamic and kinetic properties of supercooled water simulated using the iAMOEBA water model, scripts for running simulations of supercooled water, and scripts for performing trajectory analysis including using the SSSI order parameter.

References

(1) Mishima, O.; Calvert, L.; Whalley, E. An apparently first-order transition between two amorphous phases of ice induced by pressure. *Nature* **1985**, *314*, 76–78.

(2) Winkel, K.; Seidl, M.; Loerting, T.; Bove, L.; S., I.; Molinero, V.; Bruni, F.; Mancinelli, R.; Ricci, M. Structural study of low concentration LiCl aqueous solutions in the liquid, supercooled, and hyperquenched glassy states. *J Chem Phys.* **2011**, *134*, 024515.

(3) Rosu-Finsen, A.; Chikani, B.; Salzmann, C. G. Thermal desorption of H2O ice: from nanoscale films to the bulk. *MNRAS* **2022**, *517*, 1919–1927.

(4) Poole, P.; Sciortino, F.; Essmann, U.; Stanley, H. E. Phase behaviour of metastable water. *Nature* **1992**, *360*, 324–328.

(5) Debenedetti, P. G. Supercooled and glassy water. *J. Phys.: Condens. Matter* **2003**, *15*, R1669–R1726.

(6) Fitzner, M.; Sosso, G. C.; Cox, S. J.; Michaelides, A. Ice is born in low-mobility regions of supercooled liquid water. *Proc. Natl. Acad. Sci. U.S.A.* **2019**, *116*, 2009–2014.

(7) Xue, H.; Fu, Y.; Lu, Y.; Hao, D.; Li, K.; Bai, G.; Ou-Yang, Z.-C.; Wang, J.; Zhou, X. Spontaneous Freezing of Water between 233 and 235 K Is Not Due to Homogeneous Nucleation. *J. Am. Chem. Soc.* **2021**, *143*, 13548–13556.

(8) Sellberg, J. A. et al. Ultrafast X-ray probing of water structure below the homogeneous ice nucleation temperature. *Nature* **2014**, *510*, 381–384.

(9) Esmaeildoost, N. et al. Anomalous temperature dependence of the experimental x-ray structure factor of supercooled water. *J. Chem. Phys.* **2021**, *155*, 214501.

(10) K., A.-W.; Gainaru, C.; Handle, P. H.; Loerting, T. Water's second glass transition. *Proc. Natl. Acad. Sci. U.S.A.* **2013**, *110*, 17720–17725.

(11) Kringle, L.; Thornley, W. A.; Kay, B. D.; Kimmel, G. A. Reversible structural transformations in supercooled liquid water from 135 to 245 K. *Science* **2020**, *369*, 1490–1492.

(12) Neophytou, A.; Chakrabarti, D.; Sciortino, F. Topological nature of the liquid–liquid phase transition in tetrahedral liquids. *Nat. Phys.* **2022**, *18*, 1248–1253.

(13) Stillinger, F. H.; Rahman, A. Improved simulation of liquid water by molecular dynamics. *J. Chem. Phys.* **1974**, *60*, 1545–1557.

(14) Kesselring, T. A.; Franzese, G.; Buldyrev, S. V.; Herrman, H. J.; Stanley, H. E. Nanoscale Dynamics of Phase Flipping in Water near its Hypothesized Liquid-Liquid Critical Point. *Sci. Rep.* **2012**, *2*.

(15) Poole, P. H.; Bowles, R. K.; Saika-Voivod, I.; Sciortino, F. Free energy surface of ST2 water near the liquid-liquid phase transition. *J. Chem. Phys.* **2013**, *138*, 034505.

(16) Jorgensen, W. L.; Chandrasekhar, J.; Madura, J. D.; Impey, R. W.; Klein, M. L. Comparison of simple potential functions for simulating liquid water. *J. Chem. Phys.* **1983**, *79*, 926–935.

(17) Abascal, J. L. F.; Vega, C. A general purpose model for the condensed phases of water: TIP4P/2005. *J. Chem. Phys.* **2005**, *123*, 234505.

(18) Abascal, J. L. F.; Sanz, E.; García Fernández, R.; Vega, C. A potential model for the study of ices and amorphous water: TIP4P/Ice. *J. Chem. Phys.* **2005**, *122*, 234511.

(19) Palmer, J. C.; Martelli, F.; Liu, Y.; Car, R.; Panagiotopoulos, A. Z.; Debenedetti, P. G. Metastable liquid–liquid transition in a molecular model of water. *Nature* **2014**, *510*, 385–388.

(20) Smart, A. G. The war over supercooled water. **2018**,

(21) Palmer, J. C.; Poole, P. H.; Sciortino, F.; Debenedetti, P. G. Advances in Computational Studies of the Liquid–Liquid Transition in Water and Water-Like Models. *Chem. Rev.* **2018**, *118*, 9129–9151.

(22) Debenedetti, P. G.; Sciortino, F.; Zerze, G. H. Second critical point in two realistic models of water. *Science* **2020**, *369*, 289–292.

(23) Jedrecy, A.; Saitta, A. M.; Pietrucci, F. Free energy calculations and unbiased molecular dynamics targeting the liquid–liquid transition in water no man's land. *J. Chem. Phys.* **2023**, *158*, 014502.

(24) Eltareb, A.; Lopez, G. E.; Giovambattista, N. Evidence of a liquid–liquid phase transition in H2O and D2O from path-integral molecular dynamics simulations. *Sci Rep* **2022**, *12*, 6004.

(25) Weis, J.; Sciortino, F.; Panagiotopoulos, A. Z.; Debenedetti, P. G. Liquid–liquid criticality in the WAIL water model. *J. Chem. Phys.* **2022**, *157*, 024502.

(26) Gartner, T. E.; Zhang, L.; Piaggi, P. M.; Car, R.; Panagiotopoulos, A. Z.; Debenedetti, P. G. Signatures of a liquid–liquid transition in an ab initio deep neural network model for water. *Proc Natl Acad Sci USA* **2020**, *117*, 26040–26046.

(27) Gartner, T. E.; Piaggi, P. M.; Car, R.; Panagiotopoulos, A. Z.; Debenedetti, P. G. Liquid-Liquid Transition in Water from First Principles. *Phys. Rev. Lett.* **2022**, *129*, 255702.

(28) Challa, M. S. S.; Landau, D. P.; Binder, K. Finite-size effects at temperature-driven first-order transitions. *Phys. Rev. B* **1986**, *34*, 1841–1852.

(29) Piaggi, P. M.; Panagiotopoulos, A. Z.; Debenedetti, P. G.; Car, R. Phase Equilibrium of Water with Hexagonal and Cubic Ice Using the SCAN Functional. *J. Chem. Theory Comput.* **2021**, *17*, 3065–3077.

(30) Wang, L.-P.; Head-Gordon, T.; Ponder, J. W.; Ren, P.; Chodera, J. D.; Eastman, P. K.; Martinez, T. J.; Pande, V. S. Systematic Improvement of a Classical Molecular Model of Water. *J. Phys. Chem. B* **2013**, *117*, 9956–9972.

(31) Pathak, H.; Palmer, J. C.; Schlesinger, D.; Wikfeldt, K. T.; Sellberg, J. A.; Pettersson, L. G. M.; Nilsson, A. The structural validity of various thermodynamical models of supercooled water. *J. Chem. Phys.* **2016**, *145*, 134507.

(32) Pathak, H.; Spah, A.; Amann-Winkel, K.; Perakis, F.; Kim, K. K. H.; Nilsson, A. Temperature dependent anomalous fluctuations in water: shift of 1 kbar between experiment and classical force field simulations. *Mol. Phys.* **2019**, *117*, 3232–3240.

(33) Shi, R.; Tanaka, H. The anomalies and criticality of liquid water. *Proc. Natl. Acad. Sci. U.S.A.* **2020**, *117*, 26591–26599.

(34) Kringle, L.; Kay, B. D.; Kimmel, G. A. Dynamic Heterogeneity and Kovacs' Memory Effects in Supercooled Water. *J. Phys. Chem. B* **2023**, *127*, 3919–3930.

(35) Lynden-Bell, R. M.; Debenedetti, P. G. Computational Investigation of Order, Structure, and Dynamics in Modified Water Models. *J. Phys. Chem. B* **2005**, *109*, 6527–6534.

(36) Cuthbertson, M. J.; Poole, P. H. Mixturelike Behavior Near a Liquid-Liquid Phase Transition in Simulations of Supercooled Water. *Phys. Rev. Lett.* **2011**, *106*, 115706.

(37) Martelli, F.; Leoni, F.; Sciortino, F.; Russo, J. Connection between liquid and non-crystalline solid phases in water. *J. Chem. Phys.* **2020**, *153*, 104503.

(38) Donkor, E. D.; Offei-Danso, A.; Rodriguez, A.; Sciortino, F.; Hassanali, A. Beyond Local Structures In Critical Supercooled Water Through Unsupervised Learning. 2024.

(39) Malosso, C.; Manko, N.; Izzo, M. G.; Baroni, S.; Hassanali, A. Evidence of ferroelectric features in low-density supercooled water from ab initio deep neural-network simulations. 2024.

(40) Martoňák, R.; Donadio, D.; Parrinello, M. Polyamorphism of Ice at Low Temperatures from Constant-Pressure Simulations. *Phys. Rev. Lett.* **2004**, *92*, 225702.

(41) Ladd, A.; Woodcock, L. Triple-point coexistence properties of the lennard-jones system. *Chemical Physics Letters* **1977**, *51*, 155–159.

(42) Morris, J.; Song, X. The melting lines of model systems calculated from coexistence simulations. *JOURNAL OF CHEMICAL PHYSICS* **2002**, *116*, 9352–9358.

(43) García Fernández, R.; Abascal, J. L. F.; Vega, C. The melting point of ice Ih for common water models calculated from direct coexistence of the solid-liquid interface. *The Journal of Chemical Physics* **2006**, *124*, 144506.

(44) Watanabe, H.; Ito, N.; Hu, C.-K. Phase diagram and universality of the Lennard-Jones gas-liquid system. *The Journal of Chemical Physics* **2012**, *136*, 204102.

(45) Cordeiro, M.; D.S., N. Interfacial Tension Behaviour of Water/Hydrocarbon Liquid–Liquid Interfaces: A Molecular Dynamics Simulation. *Mol. Simul.* **2003**, *29*, 817–827.

(46) Zhang, Y.; Khodadadi, J. M. Ice-water interfacial energy between 235.35 and 237.15 K deduced from homogeneous nucleation rate. *Curr. Appl. Phys.* **2016**, *16*, 534–538.

(47) Willard, A. P.; Chandler, D. Instantaneous Liquid Interfaces. *J. Phys. Chem. B* **2010**, *114*, 1954–1958.

(48) Rasaiah, J. C.; Garde, S.; Hummer, G. Water in Nonpolar Confinement: From Nanotubes to Proteins and Beyond*. *Annual Review of Physical Chemistry* **2008**, *59*, 713–740.

(49) Persson, E.; Halle, B. Cell water dynamics on multiple time scales. *Proceedings of the National Academy of Sciences* **2008**, *105*, 6266–6271.

(50) Nada, H.; Furukawa, Y. Antifreeze proteins: computer simulation studies on the mechanism of ice growth inhibition. *Polymer Journal* **2012**, *44*, 690–698.

(51) Powell-Palm, M. J.; Rubinsky, B.; Sun, W. Freezing water at constant volume and under confinement. *COMMUNICATIONS PHYSICS* **2020**, *3*.

(52) Mohammed, S.; Asgar, H.; Deo, M.; Gadikota, G. Interfacial and Confinement-Mediated Organization of Gas Hydrates, Water, Organic Fluids, and Nanoparticles for the Utilization of Subsurface Energy and Geological Resources. *Energy & Fuels* **2021**, *35*, 4687–4710.

(53) Lamoureux, G.; Roux, B. Modeling induced polarization with classical Drude oscillators: Theory and molecular dynamics simulation algorithm. *J. Chem. Phys.* **2003**, *119*, 3025–3039.

(54) Albaugh, A.; Demerdash, O.; Head-Gordon, T. An efficient and stable hybrid extended Lagrangian/self-consistent field scheme for solving classical mutual induction. *J. Chem. Phys.* **2015**, *143*, 174104.

(55) Simmonett, A. C.; Pickard, I., Frank C.; Shao, Y.; Cheatham, I., Thomas E.; Brooks, B. R. Efficient treatment of induced dipoles. *J. Chem. Phys.* **2015**, *143*, 074115.

(56) Lemkul, J. A.; Roux, B.; van der Spoel, D.; MacKerell Jr., A. D. Implementation of extended Lagrangian dynamics in GROMACS for polarizable simulations using the classical Drude oscillator model. *J. Comput. Chem.* **2015**, *36*, 1473–1479.

(57) Albaugh, A.; Tuckerman, M. E.; Head-Gordon, T. Combining Iteration-Free Polarization with Large Time Step Stochastic-Isokinetic Integration. *J. Chem. Theory Comput.* **2019**, *15*, 2195–2205.

(58) Sivak, D. A.; Chodera, J. D.; Crooks, G. E. Time Step Rescaling Recovers Continuous-Time Dynamical Properties for Discrete-Time Langevin Integration of Nonequilibrium Systems. *J. Phys. Chem. B* **2014**, *118*, 6466–6474.

(59) Ren, P.; Ponder, J. W. Polarizable Atomic Multipole Water Model for Molecular Mechanics Simulation. *J. Chem. Phys. B* **2003**, *107*, 5933–5947.

(60) Basconi, J. E.; Shirts, M. R. Effects of Temperature Control Algorithms on Transport Properties and Kinetics in Molecular Dynamics Simulations. *J. Chem. Theory. Comput.* **2013**, *9*, 2887–2899.

(61) Eastman, P.; Swails, J.; Chodera, J. D.; McGibbon, R. T.; Zhao, Y.; Beauchamp, K. A.; Wang, L.-P.; Simmonett, A. C.; Harrigan, M. P.; Stern, C. D.; Wiewiora, R. P.; Brooks, B. R.; Pande, V. S. OpenMM 7: Rapid development of high performance algorithms for molecular dynamics. *PLoS Comput. Biol.* **2017**, *13*, 1–17.

Supplementary Files

This is a list of supplementary files associated with this preprint. Click to download.

- suppinfo.pdf